Enhanced *in vivo*-imaging in fish by optimized anaesthesia, fluorescent protein selection and removal of pigmentation

Short title:

Enhancing *in vivo*-imaging in fish

Colin Q. Lischik[1,2], Leonie Adelmann[1], Joachim Wittbrodt[1*]

[1] Centre for Organismal Studies (COS) Heidelberg, Heidelberg University, Heidelberg, Germany

[2] Heidelberg Biosciences International Graduate School, Heidelberg University, Heidelberg, Germany

[*]Corresponding author

E-mail: jochen.wittbrodt@cos.uni-heidelberg.de

Abstract

Fish are ideally suited for *in vivo*-imaging due to their transparency at early stages combined with a large genetic toolbox. Key challenges to further advance imaging are fluorophore selection, immobilization of the specimen and approaches to eliminate pigmentation.

We addressed all three and identified the fluorophores and anaesthesia of choice by high throughput time-lapse imaging. Our results indicate that eGFP and mCherry are the best conservative choices for *in vivo*-fluorescence experiments, when availability of well-established antibodies and nanobodies matters. Still, mVenusNB and mGFPmut2 delivered highest absolute fluorescence intensities *in vivo*. Immobilization is of key importance during extended *in vivo* imaging. Here, traditional approaches are outperformed by mRNA injection of α-Bungarotoxin which allows a complete and reversible, transient immobilization. In combination with fully transparent juvenile and adult fish established by the targeted inactivation of both, *oca2* and *pnp4a* via CRISPR/Cas9-mediated gene editing in medaka we could dramatically improve the state-of-the art imaging conditions in post-embryonic fish, now enabling light-sheet microscopy of the growing retina, brain, gills and inner organs in the absence of side effects caused by anaesthetic drugs or pigmentation.

Introduction

Fish (Zebrafish, *Danio rerio* [1,2]; Medaka, *Oryzias latipes*, [3,4]) have become popular model systems for *in vivo* imaging due to their transparent embryos and their extended genetic toolbox [5,6].

In contrast to the first hours of development, imaging of subsequent stages of development and adult life is obscured by increasing pigmentation and the active movements of the growing animals. Thus, the biggest challenge does not reside on the level of instrumentation, but rather within the specimen itself. They need to be tackled to fully exploit the excellent genetic toolbox. Long term

39 lineaging approaches in both species [7,8] will only deliver dynamic data on fate decisions, once
40 these challenges have been addressed.

41 This requires a systematic comparative analysis to combine the best suited fluorescent proteins *in*
42 *vivo* with an improvement of the long-term immobilisation/anaesthesia not interfering with the
43 viability of the organisms and approaches to further enhance the transparency of juvenile and adult
44 fish. All three major challenges are addressed below.

45 So far, the choice of a given fluorescent protein (FP) as a reporter or tag has often been based on a
46 subjective or pragmatic decision, rather than on quantitative comparison identifying the one best
47 suited. In order to address this, we systematically compared a library of widely used green and red
48 FPs and compared their fluorescence intensities during development upon mRNA injection in
49 medaka and zebrafish embryos.

50 For this purpose, we scored the respective fluorescence intensities over time and assessed whether a
51 given intensity of a FP is determined exclusively by its amino acid sequence or can be further
52 improved by codon optimization.

53 The second challenge was identifying a suitable means of anaesthesia for *in vivo* imaging of fish. This
54 is necessary since the standard anaesthetic, Tricaine or MS222, has been shown to only result in
55 incomplete anaesthesia accompanied by adverse effects on heart development (Culver and
56 Dickinson, 2010). Together with Tricaine, we systematically tested the anaesthesia induced by the
57 GABA modulating agent Etomidate and α-Bungarotoxin, a potent nicotinic acetylcholine receptor
58 (nAChR) inhibitor.

59 The third challenge was overcoming the optical obstructions posed by the pigmentation of eye and
60 peritoneum which prevent the efficient imaging of the underlying cells, tissues and organs. The
61 melanin-containing pigments are not only absorbing light, but are also auto-fluorescent and
62 consequently interfering with fluorescence microscopy [9]. Similarly, the light reflecting properties of
63 the iridescent iridophores interfere with deep *in vivo* imaging. [9]. Both represent a challenge for

64 light microscopy, in particular true for light-sheet microscopy, where the illumination axis is
65 positioned perpendicular to the detection axis [1,2]. Retinal pigmentation completely shields the eye
66 and pigmentation of the head interferes imaging of the brain or any other cranial structure. The most
67 widely used method to suppress the formation of pigment in developing teleost embryos is the
68 application of the toxic and teratogenic drug 1-phenyl 2-thiourea (PTU) [10]. While PTU prevents
69 formation of new melanin pigment, it neither abolishes already present melanin pigmentation, nor
70 blocks formation of iridophore pigment. Consequently, the limited efficacy of PTU towards
71 iridophores together with its severe and toxic side effects highlights the need for alternative
72 experimental approaches.

73 To overcome these limitations large efforts have been made to systematically breed medaka with
74 reduced pigmentation, suitable for *in vivo* imaging [11,12]. However, since these lines were
75 established by combining several different gamma-ray induced mutant alleles affecting
76 pigmentation, the resulting individuals, mutant in five different loci, are severely affected in life span
77 and fecundity and are consequently challenging to maintain [12]. In order to eliminate pigmentation
78 and light reflection in any genetic background without the need for extensive breeding we devised a
79 CRISPR/Cas9-based knockout strategy to establish pigment-free lines in any background by the
80 parallel targeted inactivation of *oca2* and *pnp4a*. This highly efficient strategy is even applicable for
81 transient approaches upon microinjection.

82 Taken together, the combination of the approaches presented in this study (double pigment
83 knockout, *α-Bungarotoxin mRNA*, *eGFP* and *H2A-mCherry*) facilitated the imaging of post-embryonic
84 medaka with a MuVi-SPIM (Multiview selective plane illumination microscope) [13,14] highlighting
85 their immediate impact.

Results

mVenNB and mCherry are the most intense fluorescent proteins in medaka

In order to assess the fluorescence intensity of different, commonly used FPs (CFP, Clover, eGFP, eGFPvar, eGFPvarA206K, Venus, YFP, mGFPmut2, mVenusNB), we performed a transient ratio-metric approach over extended periods of time. To do so we co-injected equimolar amounts of mRNAs encoding the respective green FP along with the mRNA encoding mCherry as reference. Embryos were injected at the one-cell stage and placed into a 96 well plate for imaging immediately after injection. We determined green and read fluorescence intensities every 20 minutes for at least 40 h at 28°C (exact timeframes are listed in S2 Table). We confirmed that the chorion does not negatively impact on the analysis of injected embryos by comparing embryos with and without chorion at 2, 3 and 4 dpf under the conditions detailed above. This analysis showed no interference of the chorion the determination of the fluorescence properties (Fig 1F, S1 Fig).

Fig 1. The brightest fluorescent proteins tested in medaka are mVenusNB in the green channel and mCherry in the red channel. (A) Embryos were injected with a green fluorescent protein mRNA to be tested and mCherry mRNA or with eGFP mRNA and a red fluorescent protein mRNA to be tested (1-cell stage modified from [15]). Embryos were mounted in a 96-well plate immediately after injection and automatically imaged for at least 40 h. These data were analysed semi-automated in Fiji and R. Therefore, the raw data were masked and cropped to exclude background. Subsequently, the injection volume was normalized per well by dividing with the value of the control channel at 10 hours post-fertilization. These values were plotted along their biological replicates in R. (B) Schematic overview of fluorescence intensity at 10 hpf, ordered by fluorescence intensity. The lookup table is indicated on the top of the panel, the green fluorescent proteins are shown on the left hand side and

110 the red fluorescent proteins are shown on the right hand side (embryos modified from [15]). (C)
111 Green fluorescent protein fluorescence comparison over time. Plotted is the fluorescence normalized
112 to mCherry per well against the hours post fertilization. Plates were normalized by internal control
113 for fusion of graphs (eGFP). (D) Red fluorescent protein fluorescence comparison over time. Plotted
114 is the fluorescence normalized to eGFP per well against the hours post fertilization. Plates were
115 normalized to internal control for fusion of graphs (mCherry). (E) Verification of previous results by *in*
116 *vivo*-microscopy of hatched medaka embryos (8dpf) in a light-sheet microscope, comparing the
117 fluorescence intensity of different fluorescent proteins (asterisks indicate P-values: **** P <= 0.0001,
118 *** P <= 0.001, ** P <= 0.01, * P <= 0.05, ns P > 0.05). (F) The influence of the chorion on
119 fluorescence intensity. Exemplary shown are eGFP and mCherry. There is a negligible influence of the
120 chorion of fluorescence intensity measurement. Further information can be found in S1 Fig.

121

122 Subsequently, embryos were demounted and image data were analysed in a semi-automated
123 manner by Fiji and R scripts (Fig 1A). In brief we determined the fluorescence intensities by first
124 automatically segmenting the outline of the embryo, followed by the extraction of the mean, median
125 and standard deviation of the resulting region of interest defined by the embryonic outline. The
126 values were normalized to the mean value of the reference mCherry fluorescence intensity at 10
127 hours post fertilization (hpf). For red fluorescent proteins (mCherry, mRFP, mRuby2, tagRFP, mRFP1*,
128 mScarlet-I), we used eGFP as ratiometric reference and performed an analogous analysis. The
129 resulting fluorescence intensities were ordered allowing instant comparison (Fig 1B). Our systematic
130 analysis revealed that mVenNB and mCherry show the highest fluorescent intensities *in vivo* (Fig 1).
131 We validated particularly high and low scoring candidates by high resolution imaging of mRNA
132 injected embryos at 8dpf in a selective plane illumination microscope (SPIM) (Fig 1E). This analysis
133 confirmed the initial assessments and underscores the impact of autofluorescence of pigment cells.

134 Previously Balleza and colleagues compared *in vitro* parameters to *in vivo* fluorescence in *E. coli* in
135 order to identify parameters predictive for *in vivo* fluorescence [16]. In order to assess whether this

136 holds also true for vertebrate systems we compared the fluorescence intensities obtained for the
137 different FPs above to their results (Fig 2A). Most FPs show a similar relative fluorescence intensity
138 compared to the normalization value in *E. coli* and *O. latipes*. However, some particularly intense
139 fluorescent proteins such as *mCherry* and *mVenNB* are prominently diverging from the predicted
140 parameters, underpinning the need of an *in vivo* assay to validate novel FPs in the model organism of
141 choice. Similar findings were reported from *C. elegans*, where the *in vitro* parameters are not a
142 sufficient predictor for *in vivo* fluorescence [17].

143

144 **Fig 2. Codon adaptation of *eGFP* for medaka is not improving fluorescence.** (A) Relative comparison
145 of *in vivo* fluorescence in medaka with *in vivo* fluorescence in *E. coli*. Indicated are red, green and
146 yellow fluorescent proteins and a diagonal line for orientation. While many of the fluorescent
147 proteins have similar properties, some are significantly different, reinforcing the need of a systematic
148 review of fluorescent proteins in medaka. (B) Codon adaptation indices (CAI) of all prior used
149 sequences. Codon adaptation index of each sequence is plotted for medaka and human along with a
150 diagonal line for orientation. Labelled are the two normalizing fluorescent proteins eGFP and
151 mCherry, and the outlier mRuby2. For a plot with full labelling, refer to S2 Fig. (C) Pure codon usage
152 table driven codon averaging does not improve fluorescence intensity of fluorescent proteins.
153 OleGFP (medaka codon-averaged eGFP) fluorescence intensity is overall lower than SceGFP (yeast
154 codon-averaged) and 25 to 30-fold lower than eGFP. (D) Codon adaptation indices of sequences used
155 in order to score for the effect of codon averaging. Additional to the prior used sequences are an
156 eGFP codon optimized for medaka (OleGFP) and an eGFP codon optimized for yeast (SceGFP).

157

158 We addressed a potential impact of protein structure or codon usage on the fluorescence intensities.
159 We first plotted the codon adaptation index (CAI) [18] for medaka and for human for each of the FP
160 sequences used (Fig 2B). To address the question experimentally, we designed codon optimized eGFP

161 for medaka (OleGFP) by OPTIMIZER [19] and plotted it along with an eGFP codon optimized for
162 *Saccharomyces cerevisiae* (SceGFP, Fig 2D). For experimental validation, both mRNAs were injected
163 into medaka embryos, each together with *mCherry* mRNA as injection control and compared to an
164 *eGFP* mRNA control injection. Analysis was performed as described above. The results indicate that
165 codon averaging does not improve the fluorescence intensity. In contrast, the fluorescence intensity
166 of OleGFP is even lower than that of SceGFP, hinting at inefficient translation in case of the codon
167 optimized mRNA (Fig 2C). Taken together, those experiments and the overall similar temporal
168 intensity patterns of all FPs assayed are reflecting a comparable translation efficiency of the different
169 mRNAs and comparable stability of the resulting proteins respectively (Fig 1C-D). Codon optimization
170 does not additionally improve the respective fluorescence properties.

171 The most intense fluorescent proteins in medaka were also tested in zebrafish and analysed
172 accordingly. Embryos were visualized by the mean over all timepoints, since the trend was not
173 persistent over time (Fig 3A). Green fluorescent proteins (Fig 3B) and red fluorescent proteins (Fig
174 3C) were normalized to control injections and visualized over time. Strikingly and in contrast to
175 medaka, the trend is not persistent for all FPs, but fluorescence intensity ratios rather vary with time.
176 So, the time of the assay is of crucial importance for the choice of the optimal FP during early
177 zebrafish development.

178

179 **Fig 3. The most suitable fluorescence intensity in zebrafish varies during development.** (A)
180 Schematic overview of the mean of the tested fluorescent proteins. The lookup table is indicated at
181 the top of the panel, the green fluorescent proteins are shown on the left hand side and the red
182 fluorescent proteins are shown on the right hand side (embryos modified from [20]). (B) Green
183 fluorescent protein fluorescence comparison over time. Plotted is the fluorescence normalized to
184 mCherry per well against the hours post fertilization. Analysis was conducted as outlined in Fig 1A.
185 (C) Red fluorescent protein fluorescence comparison over time. Plotted is the fluorescence

186 normalized to eGFP per well against the hours post fertilization. Analysis was conducted as outlined
187 in Fig 1A.
188

189 α-Bungarotoxin mRNA injection most efficiently anesthetises medaka 190 embryos

191 To improve the quality of anaesthesia in medaka, different forms of anaesthesia were compared by
192 scoring movements over time. We either treated embryos with the established anaesthetic Tricaine,
193 or Etomidate or injected one cell stage embryos with mRNA encoding α-Bungarotoxin [21]. All
194 embryos were dechorionated at stage 28 [15], when uninjected embryos were treated with Tricaine,
195 Etomidate, and the respective controls (DMSO, 1xERM). To avoid position effects in the 96-well
196 plate, embryos were loaded randomly and imaged in 20 minute intervals for up to 40 hours. To
197 detect movements, we performed semi-automated image analysis in Fiji [22] and R [23] (Fig 4A). Our
198 analysis workflow delivered a quantitative readout of embryonic movement assessing the efficacy of
199 the anaesthetics (Fig 4B). Strikingly, α-Bungarotoxin was the only anaesthetic efficiently blocking
200 embryonic movement. In contrast, Tricaine and Etomidate did not anesthetize efficiently and treated
201 embryos exhibited strong movements over time (Fig 4B, S1 Movie). Importantly, *α-Bungarotoxin*
202 mediated anaesthetics was reversible and embryos demounted after the analysis eventually showed
203 startle responses, comparable to that of the control treated groups (Fig 4C). S3 Fig gives a visual
204 impression of different projection types of a single well for immediate appreciation. While projection
205 of moving embryos results in a heavy blur, α-Bungarotoxin injected embryos are still visible after
206 projection, with only growth-related movements were detected. Taken together, these results
207 indicate that only *α-Bungarotoxin* functions as effective anaesthetic over extended periods of time.
208 To assess the optimal concentration for reversible anaesthesia suitable for imaging that ensures
209 proper embryonic development, we performed microinjections with different concentrations of *α-*
210 *Bungarotoxin* (Fig 4D). We determined effective concentrations that are functional even for sensitive

211 lines with limited fecundity facilitating ongoing development and breeding microscopy. In addition
212 we addressed potential effects on cardiac functionality [21], and carefully assayed heart morphology
213 and function after extended imaging in demounted embryos (S4 Fig). Only embryos injected with *α-*
214 *Bungarotoxin* exhibited normal cardiac function and development, in contrast to the Etomidate or
215 Tricaine treated embryos where heart function was clearly affected by the treatment (S4 Fig).

216

217 **Fig 4. Anaesthesia of medaka is most efficient with α-Bungarotoxin mRNA injection.** (A) Embryos
218 were injected with eGFP mRNA or eGFP mRNA along with α-Bungarotoxin mRNA (1-cell stage
219 modified from [15]). Injected embryos and uninjected embryos were dechorionated. Uninjected
220 embryos were treated with Tricaine, Etomidate (experiments), DMSO or 1x ERM (controls). Embryos
221 were randomly loaded in a 96-well plate and imaged automatically. Plates were adjusted by starting
222 stage of imaging and fused into one dataset. Consecutively, image analysis was performed semi-
223 automatically in FIJI and R. Therefore, the difference between each timepoint n and its following
224 timepoint $n + 1$ was calculated and squared. These values were imported into R and plotted along
225 with their biological replicates. (B) Movement index of injected/treated embryos over time. Data was
226 analysed as described in A. Strikingly, only α-Bungarotoxin is completely anesthetizing the embryos
227 leading to nearly no detectable difference between the different timepoints (time resolution: 20 min,
228 n as fish per condition is indicated in the legend). (C) α-Bungarotoxin-treated embryos are catching
229 up in startle response ability. Fish were startled 10 times each and the number of responses was
230 noted. Same legend as in Fig 4B applies. (α-Bungarotoxin: n = 12 fish, mock injected: n = 5 fish, wild-
231 type control: n = 8 fish, asterisks indicate P-values: **** P <= 0.0001, *** P <= 0.001, ** P <= 0.01, *
232 P <= 0.05, ns P > 0.05). (D) Different dilutions of α-Bungarotoxin were tested in order to adjust the
233 concentration so fish would wake up after microscopy. Embryos were injected with 0, 3, 6, 12 or 25
234 ng/µl α-Bungarotoxin mRNA along with eGFP mRNA as an injection control. The number of hatched
235 embryos per condition was scored (0 ng/µl: n = 33 fish, 3 ng/µl: n = 34 fish, 6 ng/µl: n = 16 fish, 12
236 ng/µl: n = 24 fish, 25 ng/µl: n = 22 fish).

237

238 # Efficient CRISPR/Cas9-based double pigment ablation in the injected

239 generation

240 We employed the CRISPR/Cas9-system in medaka embryos [24] to co-eliminate melanophores in the
241 retina and iridophores two subtypes of pigment cells already in the injected generation. We co-
242 injected of mRNA encoding Cas9 together with sgRNAs targeting a key gene for retinal melanin
243 formation *Oca2* [25] and for the formation of light reflective iridophores, *Pnp4a* [26] to efficiently
244 target melanophores and iridophores simultaneously. Bi-allelic targeting of both loci facilitated by
245 our approach established a high rate (12.5%) of pigment free embryos (Fig 5A) suitable for
246 immediate imaging. The established mutants a fully viable and breed successfully, resulting in
247 translucent embryos and young fish (Fig 5B, S2 Movie). We named the double mutants *spooky*, due
248 to the near-invisibility in petri dishes. These pigment-free fish are amenable to whole mount imaging
249 from embryonic stages up to young adults (S5 Fig). The loss of obstructing pigments in the eye
250 facilitates imaging of the brain by light-sheet microscopy. We combined all approaches described
251 above, injected mRNA encoding the most efficient fluorophores (*eGFP* and *H2A-mCherry* mRNA) into
252 *spooky* mutant fish (*Oca2*$^{-/-}$, *Pnp4a*$^{-/-}$) anesthetized with α-Bungarotoxin and performed long-term
253 imaging of retinal and brain structures previously obstructed by pigmentation (Fig 6). The results
254 obtained underscore the importance of combining all approaches related to the specimen to move
255 whole mount *in vivo* imaging to new frontiers.

256

257 **Fig 5. The acute double pigment knockout utilizing the CRISPR/Cas9-system can be deployed in the**
258 **injected generation.** (A) Medaka zygotes were microinjected with Cas9 mRNA, sgRNA (Oca2_1),
259 sgRNA (Oca2_2) and sgRNA (Pnp4a). The ratio of the embryos suitable for imaging was determined
260 (representative examples shown). At least 12.5 % of the injected embryos were suitable for imaging
261 in the injected generation. (B) Injected medaka as shown in panel A were raised, screened and

262 imaged in F1 to compare the effects of sgRNA injection. Wild-type embryos exhibit a dense, black
263 pigment in the eyes, whereas adults additionally exhibit a non-translucent peritoneum. Fish injected
264 with sgRNAs against *oca2* and *pnp4a* show dramatic loss of pigmentation surrounding the eye and
265 the peritoneum, rendering the fish more accessible for microscopy.

266

267 Discussion

268 In medaka there is a clear trend of fluorescence intensity, which is maintained throughout the
269 imaging time, i.e. ratios between fluorescent proteins remain stable. This allows for the scoring of
270 fluorescent proteins by fluorescence intensity.

271 The GFP derived fluorescent proteins mVenNB and mGFPmut2 are ranking highest in fluorescence
272 intensity. The most popular and standard fluorescent protein, eGFP, with a considerable toolset
273 available including antibodies, nanobodies, split-GFP, etc. [27–29] only scores number three with
274 respect to fluorescence intensity. Since the eGFP toolset is likely also applicable to mVenNB and
275 mGFPmut2, the balance between necessary tools and absolute fluorescence intensity will determine
276 the final choice. In some instances, optimization and evaluation could be done *in silico* assessing e.g.
277 antibody binding sites or *in vitro* by immunostaining with antibodies or nanobodies. In addition, the
278 establishment of split fluorescent proteins may be possible. Furthermore, both fluorescent proteins
279 carry an A206K mutation, preventing dimerization making those more amenable for fusion proteins
280 [30]. In conclusion, eGFP remains a solid choice if the experiment heavily relies on secondary factors,
281 which are not entirely based on *in vivo* fluorescence readout.

282 Among the red fluorescent proteins the number one candidate in medaka is mCherry, which is not
283 only the fluorescent protein with the highest fluorescence intensity, but also with the best
284 established toolbox such as nanobodies, antibodies, etc. [31].

285 Interestingly, when comparing the measured fluorescence intensities to the theoretical values such
286 as quantum yield and excitation efficiency [32], we observed a discrepancy between measured
287 values and expected results. This might be due to the different physiological conditions inherent to
288 each model organism or underlying non-optimal excitation of fluorescent proteins by single
289 wavelengths.

290 Verification of fluorescent proteins by light-sheet microscopy [1,33] is in line with previous
291 observations. Green fluorescent proteins do differ in contrast to more prominent differences among
292 the red fluorescent proteins. Notably, after mRNA injection fluorescence intensity steadily decreases
293 during development, partially accounting for the small distribution of values. It is important to
294 consider that in transgenic lines or after endogenous tagging by CRISPR/Cas9, the most intense
295 fluorescent proteins are continuously expressed and therefore exhibit their fluorescence intensity
296 and maturation time.

297 The optimal fluorescent protein in zebrafish is not as easy to score by fluorescence intensity. This is
298 due to varying intensities depending on fluorescent protein and developmental stage of the fish.
299 Here, the choice of the optimal fluorescent protein depends on the experimental condition, including
300 the stage of embryos at the time of analysis. Given that we employed standard cassettes ensuring
301 comparable mRNA stability, this may be due to different kinetics of protein maturation and turnover,
302 affecting the quantitative measurements.

303 Strikingly, most fluorescent proteins show similar *in vivo* fluorescence after normalization in medaka
304 and *E. coli*. However, some of the tested proteins diverge from this trend, reinforcing the need for
305 testing novel fluorescent proteins specifically in the species of choice. Species specific differences
306 may arise from differences in their translational or maturation machinery, cellular pH-values or any
307 combination of components different between the cells of both species.

308 In our hands the optimization of codon usages according to establish codon usage tables does not
309 improve, but rather decreases fluorescence intensity [24]. While it had been shown previously in

310 *Ciona intestinalis* that that codon averaging can positively impact on the fluorescence intensity of
311 fluorescent proteins [34]. Our results, in contrast, show that codon-usage table driven averaging is
312 not effective in improving fluorescence intensity, and rather decreased intensity by 25- to 30-fold
313 likely due to changes in mRNA stability or translation efficiency due to repetitive codons.

314 Even though widely used for fish, the anaesthetic MS222 (Tricaine) has several drawbacks such as
315 non-complete anaesthesia and developmental cardiac defects during extended *in vivo*-imaging [35].
316 Several groups were therefore trying to supplement Tricaine with different anaesthetics such as
317 Isoflurane [36], Etomidate [37] or increasing the dosage of Tricaine itself [38]. The injection of α-
318 Bungarotoxin as alternative approach has previously been suggested for zebrafish, with apparent
319 influence on development or heart morphology [21]. An obvious concern in long-term imaging
320 experiments is the photostability of the anaesthetics. Since α-Bungarotoxin is delivered as an mRNA,
321 the resulting protein is already at the site of action and will be resynthesized proportional to the
322 amount of initially injected RNA, the number of cell division and the stability of the injected mRNA.
323 The ultimate choice of the anaesthetics to be employed finally depends on the biological process to
324 be studies. If those are affected by α-Bungarotoxin, irreversibly binding to nicotinic acetylcholine
325 receptors [21], Tricaine blocking the sodium channels in neuronal membranes [39] or Etomidate
326 potentiating GABA-receptors in the central nervous system [40] might be valid alternatives with the
327 limitations discussed above.

328 The pigment double knockout *spooky* is a valuable addition to toolbox since it is readily established in
329 any existing transgenic of mutant background overcoming time consuming complex breeding
330 schemes to re-establish the transparency of e. g. see-through medaka, homozygously mutant for 5
331 loci. Already the injected generation facilitates instant deep imaging.

332 The approaches presented here facilitate efficient and deep long-term, *in vivo* imaging of fish
333 embryos and juveniles employing fluorophores with the at best quantum yields in steady, highly
334 transparent embryos e. g. by light-sheet microscopy (Fig 6). We present a streamlined strategy for

335 the optimization of additional species-specific fluorophores and provide cross-validated reference
336 points for immediate comparison of new fluorophores developed.

337

338 **Fig 6. The established toolbox enables imaging of previously challenging organs and tissues, such as**
339 **the retina and the brain.** Using the pigment double knockout in combination with α-Bungarotoxin,
340 eGFP and mCherry coupled to histone2a the imaging was conducted in a single plane illumination
341 microscope (SPIM) we could image the head region of wild-type and *spooky* embryos. Hollow
342 arrowheads point towards the eyes in A and B. (A) Maximum projection of *H2A-mCherry* signal of a
343 lateral view of a wild-type medaka embryo. The eye is not penetrable and no nuclei are visible within
344 or behind it. (A') Maximum projection of *H2A-mCherry* signal of a lateral view of a *spooky* medaka
345 embryo. The eye is penetrable and nuclei are visible within or behind it. (B) Maximum projection of
346 *H2A-mCherry* signal of a dorsal view of a wild-type medaka embryo. The eye is not penetrable and no
347 nuclei are visible within it. (B') Maximum projection of *H2A-mCherry* signal of a dorsal view of a
348 *spooky* medaka embryo. The eye is penetrable and nuclei are visible within it. (C) Stitched maximum
349 projections of a dorsal view of a *spooky* embryo. This embryo was imaged for 48 hours, which can be
350 seen in S3 Movie.

351

352 Materials and Methods

353 Fish husbandry and microinjections

354 Medaka (*Oryzias latipes*) and zebrafish (*Danio rerio*) stocks were maintained as previously described
355 [41]. All fish are maintained in the closed stocks of COS at Heidelberg University. Fish husbandry and
356 experiments were performed according to local animal welfare standards (Tierschutzgesetz 111, Abs.
357 1, Nr. 1, Haltungserlaubnis) and in accordance with European Union animal welfare guidelines. The
358 fish facility is under the supervision of the local representative of the animal welfare agency.

359 Embryos were staged according to Iwamatsu [15]. Medaka microinjections were performed as
360 previously described [3].

361 CRISPR/Cas9 and single guide RNAs

362 JDS246 was a gift from Keith Joung (Addgene plasmid # 43861). Cas9 mRNA was transcribed by
363 mMessage mMachine Sp6 Transcription Kit (Thermo Fisher). Single guide RNAs were predicted by
364 CCTOP [24] and subsequently cloned into DR274 [42]: sgRNA(Oca2_1): GAAACCCAGGTGGCCATTGC,
365 sgRNA(Oca2_2): TTGCAGGAATCATTCTGTGT, sgRNA(Pnp4a): CCTGGGGGCGGTGCTTAGTC. DR274 was
366 a gift from Keith Joung (Addgene plasmid # 42250) [42]. The vector was linearized by DraI-digest and
367 transcribed by MEGAscript T7 transcription Kit (Thermo Fisher). All RNAs were purified by RNeasy
368 Mini Kit (Qiagen). Injected concentrations were: 150 ng/µl Cas9 mRNA and 15 ng/µl per sgRNA.

369 Loading and imaging of 96-well plates

370 96-well plates were loaded with 150 µl volume per well, including the treatment solution and the
371 embryo. The plates were loaded based on a randomized loading scheme created by a customized R
372 script, which creates a loading scheme and a table of each well for further use in the analysis. The
373 plates were sealed by a gas permeable moisture barrier seal (4ti-0516/96, 4titude, Dorking, England),
374 loaded into the ACQUIFER Imaging Machine (DITABIS, Pforzheim, Germany) and imaged for a defined
375 time and channel composition. The plates were continuously incubated at 28°C. An overview of the
376 imaged plates can be found in S2 Table along with the timeframe, timestep and used channels. A
377 general description of the imaging condition can be found in the section about the semi-automated
378 analysis of the experiment, i.e. either anaesthetic or fluorescent protein analysis.

379 The used LEDs and filters in the ACQUIFER Imaging Machine were a 470 nm LED in combination with
380 LED-FITC-A-000 (Semrock, Inc.) for the green channel and a 550 nm in combination with a LED-TRITC-
381 A-000 (Semrock, Inc.) for the red channel.

382 ## Anesthesia reagents

383 α-Bungarotoxin mRNA was transcribed from pmtb-t7-alpha-bungarotoxin, which was a gift from
384 Sean Megason (Addgene plasmid # 69542) [43]. The vector was digested by EcoRV-digest and the
385 linearized plasmid transcribed by mMessage mMachine Sp6 Transcription Kit (Thermo Fisher) for 4h.
386 The mRNA was purified with the RNeasy Mini Kit (Qiagen). Embryos were microinjected with 3-25
387 ng/µl α-Bungarotoxin mRNA along with 50 ng/µl eGFP mRNA. Embryos were then either mounted
388 into a 96-well plate for assaying anaesthesia efficiency or the number of hatched and swimming
389 embryos was scored for developmental stages.

390 Etomidate solution was prepared as a 10 mg/l solution (7.5 µl of a 4 mg/ml stock solution in DMSO in
391 3 ml 1x ERM). The DMSO solution was prepared accordingly, yielding a 0.25% DMSO solution. A
392 solution of 1x Tricaine (0.02% w/v, A5040, Sigma- Aldrich) was prepared.

393 ## Heart morphology scoring and heart rate measurements

394 Embryos were imaged for 10 seconds with 25 frames per second in order to score heart morphology
395 and heart rates at 25°C. The data was imported into R [23] and plotted using ggpubr and xlsx libraries
396 [44].

397 ## Startle-response assay

398 Demounted, with α-Bungarotoxin mRNA injected embryos and control embryos were startled with a
399 pipette tip for 10 times. The number of responses was noted and plotted in R using the ggpubr
400 library.

401 ## Fluorescent protein cloning and transcription

402 All fluorescent proteins were cloned into pGGEV3 from the Golden GateWAY toolkit [45]. Each
403 construct was cloned with a start and stop codon to ensure maximum comparability of the resulting
404 mRNAs. Fluorescent proteins were cloned from present plasmids except for the following.
405 cytoplasmic EKAR (Cerulean-Venus) was a gift from Karel Svoboda (Addgene plasmid # 18679) [46],

406 mRuby2-C1 was a gift from Michael Davidson (Addgene plasmid # 54768) [47], pcDNA3-Clover was a
407 gift from Michael Lin (Addgene plasmid # 40259) [47], pmScarlet-i_C1 was a gift from Dorus Gadella
408 (Addgene plasmid # 85044) [43] and SceGFP was a gift from Sabine Strahl [48] eGFP was codon
409 optimized for medaka by OPTIMIZER [19] resulting in the sequence of OleGFP. OleGFP was
410 synthesized by GeneArt Gene Synthesis (Thermo Fisher). Cloned plasmids were linearized with SpeI
411 prior to transcription and transcribed by mMessage mMachine Sp6 Transcription Kit (Thermo Fisher).
412 Fluorescent protein mRNA was microinjected in equimolar amounts compared to 50 ng/µl eGFP
413 mRNA.

414 SPIM image acquisition

415 Medaka embryos were anesthetized with 1x Tricaine or by α-Bungarotoxin mRNA injection and
416 stacks were acquired in a MuVi-SPIM (multiview selective plane illumination microscope) [13,14,49]
417 as described before [50] for the 25x detection setup, with the addition of a 488 nm illumination and
418 a corresponding 525/50 bandpass filter. For the measurements of fluorescence intensity the
419 resulting images were divided by the control channel, masked by the Otsu algorithm [51] and
420 subsequently measured.

421 The resulting tables were imported into R [23] and fused into one dataset. The measurements were
422 linked to conditions and plotted using ggplot2 [52]. The used R libraries were: data.table [53], zoo
423 [54], ggrepel [55], and ggpubr.

424 The stacks resulting in Fig 6 were recorded and imported into Fiji [22]. They were transformed with
425 the logarithm due to the varying expression of cell types and autofluorescence of leftover pigments.

426 Comparison of medaka and *E. coli in vivo* fluorescence intensity

427 *E. coli* values were extracted from supplementary material of Balleza et al. [16]. Medaka values were
428 calculated as a mean of all data of one fluorescent protein from 23 to 30 hpf from imaged data and

429 normalized to mRFP1* for red fluorescent proteins, eGFP for green fluorescent proteins and Venus
430 for yellow fluorescent proteins (set to a value of 1.2, according to the *E. coli* value).

431 Codon usage table driven codon averaging and adaptation index

432 Codon averaging was performed by OPTIMIZER [19], using the codon usage table, which can be
433 obtained from HIVE-CUTs [56]. Codon adaptation indices of all used sequences were scored by using
434 the seqinr library in R [57] and codon usage tables from HIVE-CUTs [56]. The data was plotted using
435 ggplot2 [52], readr [58], data.table [53], condformat [59] and ggrepel [55].

436 Semi-automated analysis anesthesia

437 One slice of each well was acquired by autofocus (16 steps with a distance of 25 µm, software-based)
438 per timepoint in brightfield with a CFI Plan Achromat UW 2x, N.A. 0.06 objective (Nikon). Illumination
439 was performed for 20 ms at an LED intensity of 100 %. The timelapse was recorded for at least 45
440 hours in 20 or 33 minute intervals. Subsequently the imaged medaka were staged for both uösed
441 plates and the timepoint 0 was set according to the higher starting stage (stage 28) in order to be
442 able to fuse the plate data. The following steps were performed in Fiji [22]. These images were
443 concatenated to a stack per well. Subsequently the square of the difference of timepoints was
444 calculated and exported as a table.

445 The resulting tables were loaded into R [23] and fused into one dataset. The negative wells (dead or
446 non-developing embryos) were dropped from the data set, the wells were linked to the
447 corresponding conditions and the data was plotted using ggplot2. The used R libraries were:
448 data.table [53] and ggplot2 [52]. Customized scripts are available through github
449 (https://git.io/fAPnh).

450 Semi-automated analysis of fluorescent proteins

451 A total of 12 z-slices with 100 µm step size were acquired with a CFI Plan Fluor 4x, N.A. 0.13 objective
452 (Nikon) per well, guaranteeing the embryo to be included in the image. These slices were acquired in

453 the previously described green and red channel. Illumination was performed for 50 ms at an LED
454 intensity of 50 % for both channels. Yellow and green fluorescent proteins were recorded in the
455 green channel due to the limitation of light-sheet microscopes of requiring the according filter. The
456 timelapse was recorded from directly after injection up to at least 40 hours for the longer
457 experiments, once each day for the 2, 3 and 4 dpf experiment and from injection to 48 hours for the
458 codon adaptation experiment. The following steps were performed in Fiji [22]. Each slice of each
459 channel was masked by both channels by applying an auto threshold with the Otsu algorithm and
460 cropping each channel by both resulting masks [51]. The resulting, masked images were measured by
461 excluding the background. All wells were checked for fluorescence at the maximum and the half-
462 maximum timepoint in order to exclude developmentally impaired or dead embryos.

463 The resulting tables were imported into R [23] and fused into one dataset. The negative wells were
464 discarded, the wells were linked to the corresponding conditions and normalized to the injection
465 control per well at 10 hpf. Used was the data masked by the channel of the injection control to
466 ensure automatic cropping. The data was plotted using ggplot2. The used R libraries were: data.table
467 [53], zoo [54], ggrepel [55] and ggplot2 [52]. Customized scripts are available through github
468 (https://git.io/fAPnh).

469 Acknowledgements

470 We thank Jochen Gehrig and ACQUIFER (DITABIS AG, Pforzheim) for cooperation on automated
471 microscopy and technical feedback. We thank Alex Cornean, Clara Becker, Tinatini Tavhelidse, Jakob
472 Gierten and Thomas Thumberger for critical reading and comments on the manuscript. We also
473 thank Dimitri Kromm and Lars Hufnagel for continuous support in light-sheet imaging. We thank Alex
474 Cornean for contributing to the schemes in Fig 1 and 4. We thank Steffen Lemke, Lars Hufnagel and
475 Thomas Höfer for critical comments on the manuscript.

476 # Competing interests

477 No competing interests declared.

478 # Funding

479 This work was supported by the German Science Foundation (DFG, SFB 1324 TP B4 to JW). The
480 funders had no role in study design, data collection and interpretation, or the decision to submit the
481 work for publication.

482 # Data availability

483 Not available, raw data used exceeds the reasonable limits of Dryad and Figshare (> 11 TB).

484 # References

485 1. Huisken J, Swoger J, Del Bene F, Wittbrodt J, Stelzer EHK. Optical sectioning deep inside live
486 embryos by selective plane illumination microscopy. Science. 2004;305: 1007–9.
487 doi:10.1126/science.1100035

488 2. Keller PJ, Schmidt AD, Santella A, Khairy K, Bao Z, Wittbrodt J, et al. Fast, high-contrast
489 imaging of animal development with scanned light sheet-based structured-illumination
490 microscopy. Nat Methods. Nature Publishing Group; 2010;7: 637–642.
491 doi:10.1038/nmeth.1476

492 3. Rembold M, Lahiri K, Foulkes NS, Wittbrodt J. Transgenesis in fish: efficient selection of
493 transgenic fish by co-injection with a fluorescent reporter construct. Nat Protoc. 2006;1:
494 1133–9. doi:10.1038/nprot.2006.165

495 4. Seleit A, Krämer I, Ambrosio E, Stolper JS, Dross N, Lischik CQ, et al. Neural stem cells induce
496 the formation of their physical niche during organogenesis. Elife. 2017; 1–30.
497 doi:http://dx.doi.org/10.1101/149955

498 5. Kirchmaier S, Naruse K, Wittbrodt J, Loosli F. The Genomic and Genetic Toolbox of the Teleost
499 Medaka (Oryzias latipes). Genetics. 2015;199: 905–918. doi:10.1534/genetics.114.173849

500 6. Driever W, Stemple D, Schier A, Solnica-Krezel L. Zebrafish: genetic tools for studying
501 vertebrate development. Trends Genet. 1994;10: 152–159. doi:https://doi.org/10.1016/0168-
502 9525(94)90091-4

503 7. Centanin L, Ander J-J, Hoeckendorf B, Lust K, Kellner T, Kraemer I, et al. Exclusive multipotency
504 and preferential asymmetric divisions in post-embryonic neural stem cells of the fish retina.
505 Development. 2014;141: 3472–3482. doi:10.1242/dev.109892

506 8. Pan YA, Freundlich T, Weissman T a, Schoppik D, Wang XC, Zimmerman S, et al. Zebrabow:
507 multispectral cell labeling for cell tracing and lineage analysis in zebrafish. Development.
508 2013;140: 2835–46. doi:10.1242/dev.094631

509 9. Fujii R. The regulation of motile activity in fish chromatophores. Pigment Cell Res. 2000;13:
510 300–319. doi:10.1034/j.1600-0749.2000.130502.x

511 10. Karlsson J, von Hofsten J, Olsson P-E. Generating Transparent Zebrafish: A Refined Method to
512 Improve Detection of Gene Expression During Embryonic Development. Mar Biotechnol.
513 2001;3: 0522–0527. doi:10.1007/s1012601-0053-4

514 11. Wakamatsu Y, Pristyazhnyuk S, Kinoshita M, Tanaka M, Ozato K. The see-through medaka : A
515 fish model that is transparent throughout life. PNAS. 2001;98: 10046–10050.

516 12. Ohshima A, Morimura N, Matsumoto C, Hiraga A, Komine R, Kimura T, et al. Effects of Body-
517 Color Mutations on Vitality : An Attempt to Establish Easy-to-Breed See-Through Medaka
518 Strains by Outcrossing. G3. 2013;3: 1577–1585. doi:10.1534/g3.113.007575

519 13. Medeiros G de, Norlin N, Gunther S, Albert M, Panavaite L, Fiuza U-M, et al. Confocal
520 multiview light-sheet microscopy. Nat Commun. Nature Publishing Group; 2015;6: 8881.
521 doi:10.1038/ncomms9881

522 14. Krzic U, Gunther S, Saunders TE, Streichan SJ, Hufnagel L. Multiview light-sheet microscope for
523 rapid in toto imaging. Nat Methods. 2012;9: 730–733. doi:10.1038/nmeth.2064

524 15. Iwamatsu T. Stages of normal development in the medaka Oryzias latipes. Mech Dev.
525 2004;121: 605–618. doi:10.1016/j.mod.2004.03.012

526 16. Balleza E, Kim JM, Cluzel P. A systematic characterization of maturation kinetics of fluorescent
527 proteins in live cells. Nat Methods. 2017;6: 1–10. doi:10.1038/nmeth.4509

528 17. Heppert JK, Dickinson DJ, Pani AM, Higgins CD, Steward A, Ahringer J, et al. Comparative
529 assessment of fluorescent proteins for in vivo imaging in an animal model system. Strome S,
530 editor. Mol Biol Cell. The American Society for Cell Biology; 2016;27: 3385–3394.
531 doi:10.1091/mbc.E16-01-0063

532 18. Puigbò P, Bravo IG, Garcia-Vallvé S. E-CAI: A novel server to estimate an expected value of
533 Codon Adaptation Index (eCAI). BMC Bioinformatics. 2008;9: 1–7. doi:10.1186/1471-2105-9-
534 65

535 19. Puigbò P, Guzmán E, Romeu A, Garcia-Vallvé S. OPTIMIZER: A web server for optimizing the
536 codon usage of DNA sequences. Nucleic Acids Res. 2007;35: 126–131.
537 doi:10.1093/nar/gkm219

538 20. Kimmel CB, Ballard WW, Kimmel SR, Ullmann B, Schilling TF. Stages of embryonic
539 development of the zebrafish. Dev Dyn an Off public. 1995;203: 253–310.
540 doi:10.1002/aja.1002030302

541 21. Swinburne IA, Mosaliganti KR, Green AA, Megason SG. Improved Long-Term Imaging of
542 Embryos with Genetically Encoded α-Bungarotoxin. PLoS One. 2015;10: e0134005.
543 doi:10.1371/journal.pone.0134005

544 22. Schindelin J, Arganda-Carreras I, Frise E, Kaynig V, Longair M, Pietzsch T, et al. Fiji: An open-
545 source platform for biological-image analysis. Nat Methods. 2012;9: 676–682.

546 doi:10.1038/nmeth.2019

547 23. R Core Team. R: A Language and Environment for Statistical Computing [Internet]. Vienna,
548 Austria; 2018. Available: https://www.r-project.org/

549 24. Stemmer M, Thumberger T, del Sol Keyer M, Wittbrodt J, Mateo JL. CCTop: An Intuitive,
550 Flexible and Reliable CRISPR/Cas9 Target Prediction Tool. PLoS One. 2015;10: e0124633.
551 doi:10.1371/journal.pone.0124633

552 25. Fukamachi S, Asakawa S, Wakamatsu Y, Shimizu N, Mitani H, Shima A. Conserved function of
553 medaka pink-eyed dilution in melanin synthesis and its divergent transcriptional regulation in
554 gonads among vertebrates. Genetics. 2004;168: 1519–1527.
555 doi:10.1534/genetics.104.030494

556 26. Kimura T, Takehana Y, Naruse K. pnp4a Is the Causal Gene of the Medaka Iridophore Mutant,
557 guanineless. G3. 2017;7: g3.117.040675. doi:10.1534/g3.117.040675

558 27. Caussinus E, Kanca O, Affolter M. Fluorescent fusion protein knockout mediated by anti-GFP
559 nanobody. Nat Struct Mol Biol. Nature Publishing Group; 2011;19: 117–121.
560 doi:10.1038/nsmb.2180

561 28. Kubala MH, Kovtun O, Alexandrov K, Collins BM. Structural and thermodynamic analysis of the
562 GFP:GFP-nanobody complex. Protein Sci. 2010;19: 2389–2401. doi:10.1002/pro.519

563 29. Kamiyama D, Sekine S, Barsi-Rhyne B, Hu J, Chen B, Gilbert LA, et al. Versatile protein tagging
564 in cells with split fluorescent protein. Nat Commun. Nature Publishing Group; 2016;7: 11046.
565 doi:10.1038/ncomms11046

566 30. Zacharias DA, Violin JD, Newton AC. Partitioning of Lipid-Modified Monomeric CFPs into
567 Membrane Microdomains of Live Cells. Science. 2002;296: 913–6.
568 doi:10.1126/science.1068539

569 31. Katoh Y, Terada M, Nishijima Y, Takei R, Nozaki S, Hamada H, et al. Overall Architecture of the

570 Intraflagellar Transport (IFT)-B Complex Containing Cluap1/IFT38 as an Essential Component
571 of the IFT-B Peripheral Subcomplex. J Biol Chem. 11200 Rockville Pike, Suite 302, Rockville,
572 MD 20852-3110, U.S.A.: American Society for Biochemistry and Molecular Biology; 2016;291:
573 10962–10975. doi:10.1074/jbc.M116.713883

574 32. Day RN, Davidson MW. The fluorescent protein palette: tools for cellular imaging. Chem Soc
575 Rev. 2009;38: 2887–2921. doi:10.1039/b901966a.The

576 33. Keller PJ, Schmidt AD, Wittbrodt J, Stelzer EHK. Reconstruction of Zebrafish Early Embryonic
577 Development by Scanned Light Sheet Microscopy. Science (80-). 2008;322: 1065–1069.
578 doi:10.1126/science.1162493

579 34. Zeller RW, Weldon DS, Pellatiro MA, Cone AC. Optimized green fluorescent protein variants
580 provide improved single cell resolution of transgene expression in ascidian embryos. Dev Dyn.
581 2006;235: 456–467. doi:10.1002/dvdy.20644

582 35. Culver JC, Dickinson ME. The effects of hemodynamic force on embryonic development.
583 Microcirculation. 2010;17: 164–178. doi:10.1111/j.1549-8719.2010.00025.x

584 36. Dray N, Bedu S, Vuillemin N, Alunni A, Coolen M, Krecsmarik M, et al. Large-scale live imaging
585 of adult neural stem cells in their endogenous niche. Development. 2015;142: 3592–3600.
586 doi:10.1242/dev.123018

587 37. Readman GD, Owen SF, Knowles TG, Murrell JC. Species specific anaesthetics for fish
588 anaesthesia and euthanasia. Sci Rep. Springer US; 2017;7: 7102. doi:10.1038/s41598-017-
589 06917-2

590 38. Barbosa JS, Sanchez-gonzalez R, Di Giaimo R, Baumgart EV, Theis FJ, Götz M, et al. Live
591 imaging of adult neural stem cell behavior in the intact and injured zebrafish brain. Science.
592 2015;348: 789–93. doi:10.5061/dryad.hq4v0.SUPPLEMENTARY

593 39. Frazier DT, Narahashi T. Tricaine (MS-222): Effects on ionic conductances of squid axon

594 membranes. Eur J Pharmacol. 1975;33: 313–317. doi:10.1016/0014-2999(75)90175-2

595 40. Reynolds DS, Rosahl TW, Cirone J, O'Meara GF, Haythornthwaite A, Newman RJ, et al.
596 Sedation and Anesthesia Mediated by Distinct GABAA Receptor Isoforms. J Neurosci. 2003;23:
597 8608 LP-8617. Available: http://www.jneurosci.org/content/23/24/8608.abstract

598 41. Koster R, Stick R, Loosli F, Wittbrodt J. Medaka spalt acts as a target gene of hedgehog
599 signaling. Development. 1997;124: 3147–3156.

600 42. Hwang WY, Fu Y, Reyon D, Maeder ML, Tsai SQ, Sander JD, et al. Efficient genome editing in
601 zebrafish using a CRISPR-Cas system. Nat Biotechnol. Nature Publishing Group, a division of
602 Macmillan Publishers Limited. All Rights Reserved.; 2013;31: 227. Available:
603 http://dx.doi.org/10.1038/nbt.2501

604 43. Bindels DS, Haarbosch L, van Weeren L, Postma M, Wiese KE, Mastop M, et al. mScarlet: a
605 bright monomeric red fluorescent protein for cellular imaging. Nat Methods. Nature
606 Publishing Group, a division of Macmillan Publishers Limited. All Rights Reserved.; 2016;14:
607 53. Available: http://dx.doi.org/10.1038/nmeth.4074

608 44. Dragulescu AA. xlsx: Read, write, format Excel 2007 and Excel 97/2000/XP/2003 files
609 [Internet]. 2014. Available: https://cran.r-project.org/package=xlsx

610 45. Kirchmaier S, Lust K, Wittbrodt J. Golden GATEway Cloning - A Combinatorial Approach to
611 Generate Fusion and Recombination Constructs. PLoS One. 2013;8: e76117.
612 doi:10.1371/journal.pone.0076117

613 46. Harvey CD, Ehrhardt AG, Cellurale C, Zhong H, Yasuda R, Davis RJ, et al. A genetically encoded
614 fluorescent sensor of ERK activity. Proc Natl Acad Sci U S A. 2008;105: 19264–19269.
615 doi:0804598105 [pii]\r10.1073/pnas.0804598105

616 47. Lam AJ, St-pierre F, Gong Y, Marshall JD, Cranfill PJ, Baird MA, et al. Improving FRET dynamic
617 range with bright green and red fluorescent proteins. Nat Methods. 2012;9: 1005–1012.

618 doi:10.1038/NMETH.2171

619 48. Xu C, Wang S, Thibault G, Ng DTW. Futile Protein Folding Cycles in the ER Are Terminated by
620 the Unfolded Protein O-Mannosylation Pathway. Science (80-). 2013;340: 978–982.
621 doi:10.1126/science.1234055

622 49. Tomer R, Khairy K, Amat F, Keller PJ. Quantitative high-speed imaging of entire developing
623 embryos with simultaneous multiview light-sheet microscopy. Nat Methods. Nature
624 Publishing Group; 2012;9: 755–763. doi:10.1038/nmeth.2062

625 50. Caroti F, Gonzalez Avalos E, Noeske V, Gonzalez Avalos P, Kromm D, Wosch M, et al.
626 Decoupling from yolk sac is required for extraembryonic tissue spreading in the scuttle fly
627 Megaselia abdita. bioRxiv. 2017; 1–34.

628 51. Otsu N. A threshold selection method from gray level histograms. {IEEE} Trans Syst Man
629 Cybern. 1979;9: 62–66.

630 52. Wickham H. ggplot2: Elegant Graphics for Data Analysis [Internet]. Springer-Verlag New York;
631 2009. Available: http://ggplot2.org

632 53. Dowle M, Srinivasan A. data.table: Extension of `data.frame` [Internet]. 2017. Available:
633 https://cran.r-project.org/package=data.table

634 54. Zeileis A, Grothendieck G. zoo: S3 Infrastructure for Regular and Irregular Time Series. J Stat
635 Softw. 2005;14: 1–27. doi:10.18637/jss.v014.i06

636 55. Slowikowski K. ggrepel: Repulsive Text and Label Geoms for “ggplot2” [Internet]. 2017.
637 Available: https://cran.r-project.org/package=ggrepel

638 56. Athey J, Alexaki A, Osipova E, Rostovtsev A, Santana-Quintero L V., Katneni U, et al. A new and
639 updated resource for codon usage tables. BMC Bioinformatics. BMC Bioinformatics; 2017;18:
640 1–10. doi:10.1186/s12859-017-1793-7

641 57. Charif D, Lobry JR. Seqin{R} 1.0-2: a contributed package to the {R} project for statistical

642 computing devoted to biological sequences retrieval and analysis. In: Bastolla U, Porto M,
643 Roman HE, Vendruscolo M, editors. Structural approaches to sequence evolution: Molecules,
644 networks, populations. New York: Springer Verlag; 2007. pp. 207–232.

645 58. Wickham H, Hester J, Francois R. readr: Read Rectangular Text Data [Internet]. 2017.
646 Available: https://cran.r-project.org/package=readr

647 59. Oller Moreno S. condformat: Conditional Formatting in Data Frames [Internet]. 2017.
648 Available: https://cran.r-project.org/package=condformat

649

650 Supporting information

651

652 **S1 Fig. Wild-type vs. dechorionated fluorescence extraction.** Embryos were injected as previously
653 mentioned. Half of each condition was dechorionated. Both conditions were imaged at 2, 3 and 4dpf
654 and compared to each other. Optical properties of the chorion were negligible and therefore
655 neglected in the analysis since dechorionation has a larger impact on development, especially when
656 performed in an early stage (2-4 dpf).

657

658 **S2 Fig. Codon adaptation indices of all used sequences.** Codon adaptation index of each sequence is
659 plotted for medaka and human along with a diagonal line for orientation.

660

661 **S3 Fig. Single well projections along time.** Single wells were projected with three different projection
662 types along time: standard deviation, average projection. In case the embryos are not moving it is to
663 be expected to see the full contours of the embryo in the standard deviation and in the average

664 projection. This is not the case for most of the conditions, except for the α-Bungarotoxin mRNA
665 injected embryo.

666

667 **S4 Fig. Injections of α-Bungarotoxin have no detectable impact on heart development.** (A) Embryos
668 after demounting from the 96-well plate and finishing the assay (stage 31). No cardiac defects are
669 visible in both controls and embryos injected with α-Bungarotoxin mRNA. For Tricaine, mild defects
670 can be detected, whereas severe defects can be observed in Etomidate treated embryos. (B) Heart
671 rate of α-Bungarotoxin is statistically indistinguishable to its control (mock injection). Mild defects
672 and changes can be observed in Tricaine and Etomidate treated embryos (asterisks indicate P-values:
673 **** P <= 0.0001, *** P <= 0.001, ** P <= 0.01, * P <= 0.05, ns P > 0.05). (C) Different dilutions of α-
674 Bungarotoxin were tested in order to adjust the concentration so fish would wake up after
675 microscopy. Embryos were injected with 0, 3, 6, 12 or 25 ng/µl α-Bungarotoxin mRNA along with
676 eGFP mRNA as an injection control. The number of hatched embryos and the number of swimming
677 embryos per condition was scored (0 ng/µl: n = 33 fish, 3 ng/µl: n = 34 fish, 6 ng/µl: n = 16 fish, 12
678 ng/µl: n = 24 fish, 25 ng/µl: n = 22 fish).

679

680 **S5 Fig. Adult medaka with pigment knockout.** Addition to Fig 5B. Stage 27, hatched and juvenile fish
681 of the wild-type strain and the double pigment knockout line were imaged. In addition, *oca2*$^{-/-}$ fish
682 are shown at stage 36 and adult.

683

684 **S1 Movie. Embryos with different anesthetics.** Collection of embryos used in the analysis of Fig 4B.
685 Color code is matching the color code in Fig 4.

686 **S2 Movie. Development of a wild-type and mutant embryo.** Development of a wild-type and a *oca2*$^{-}$
687 $^{/-}$ pigment knockout embryo.

688 **S3 Movie. A developing spooky embryo.** Stitched stacks of a developing *spooky* embryo, injected
689 with with *α-Bungarotoxin*, *eGFP* and *mCherry* coupled to *histone2a.* The imaging time was 48 hours
690 and the time interval 1 hour between the stacks.

691 **S1 Table. Fluorescent proteins used in this study.** All fluorescent proteins used throughout this work
692 including addgene identifiers for comparisons, sequences and mutations from ancestor fluorescent
693 proteins. Furthermore, fluorescent proteins were compared to the classification in the recent
694 publication of Balleza et al., where they made an effort to distinguish the different fluorescent
695 protein versions [16].

696 **S2 Table. All plates analyzed for this study.**

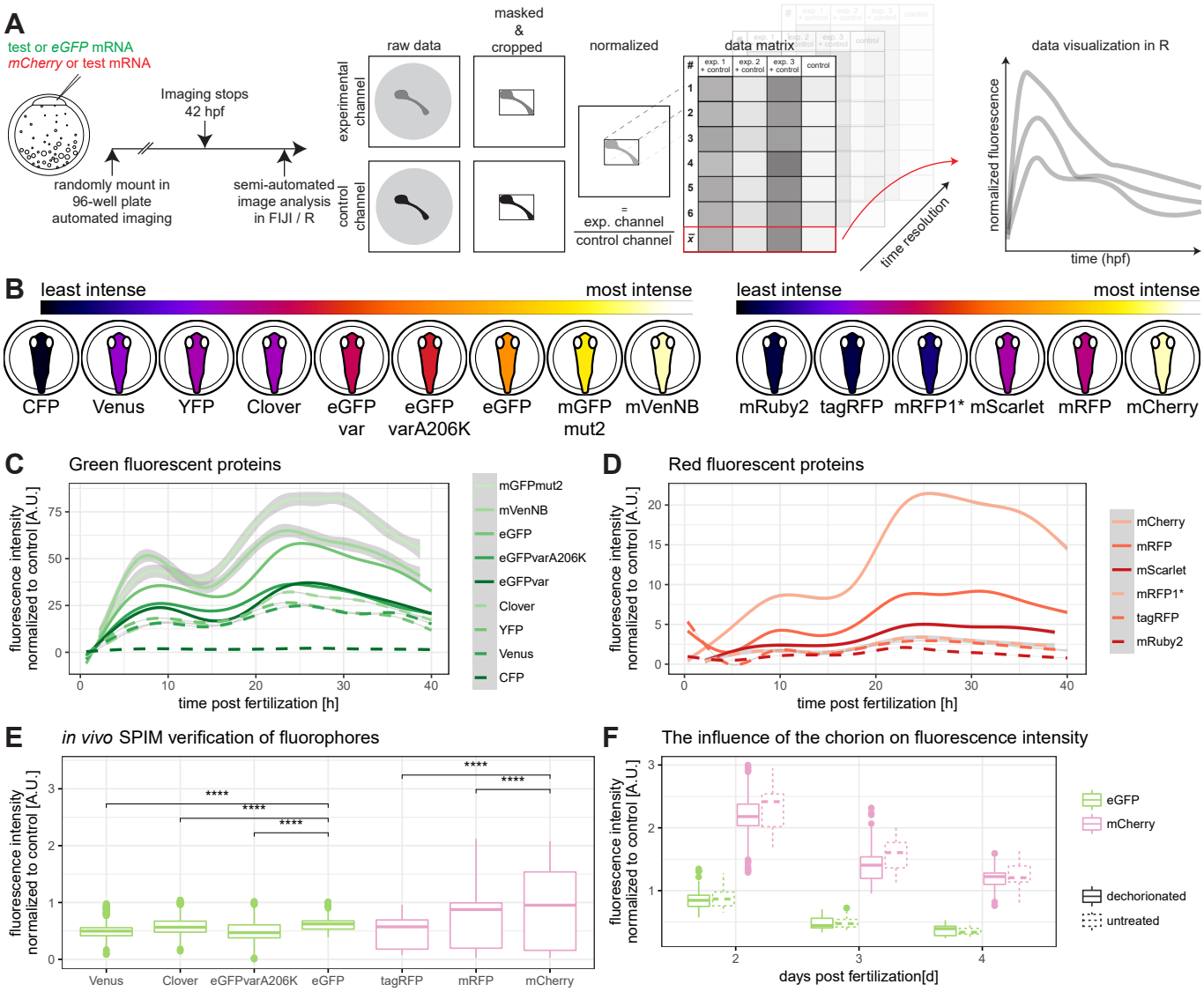

Fig 1, Lischik et al. 2018

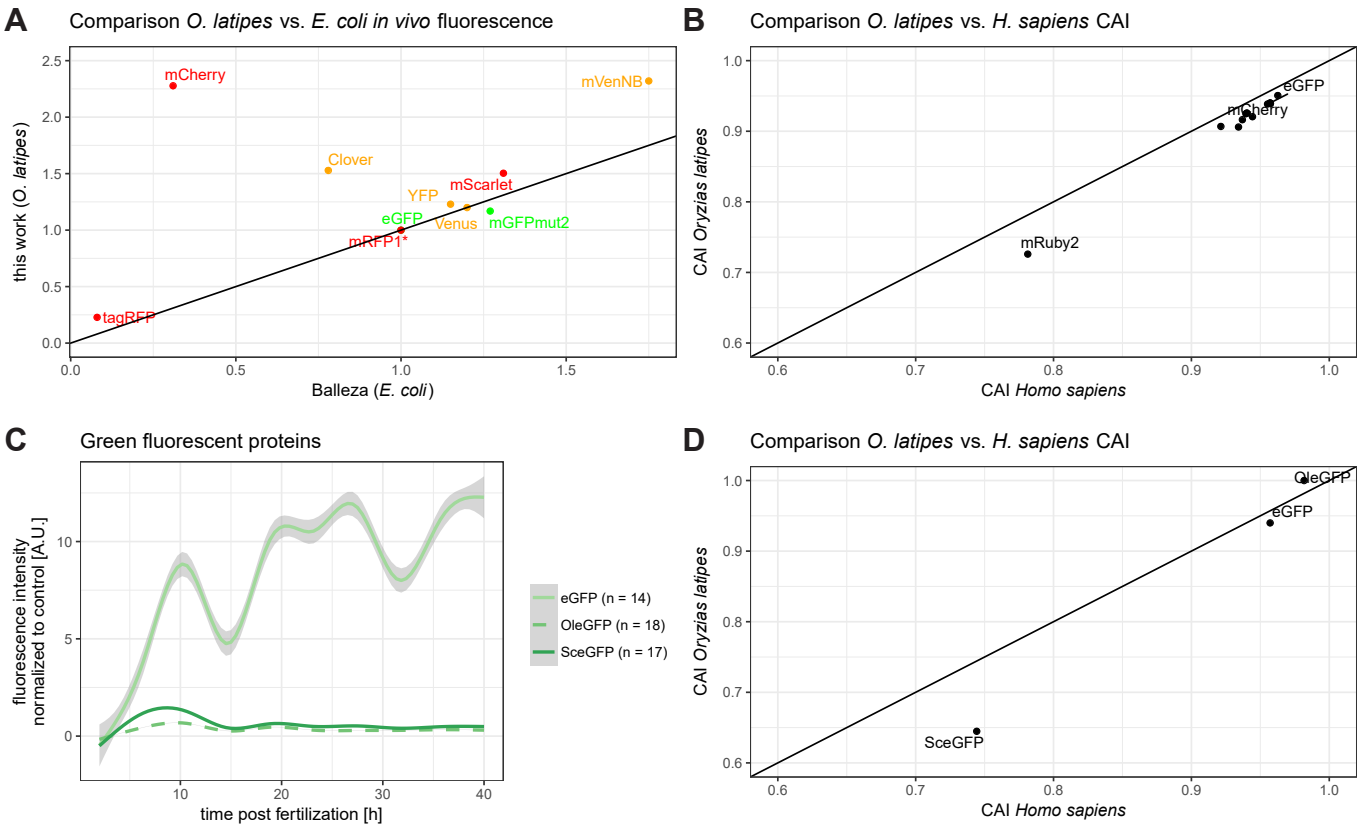

Fig 2, Lischik et al. 2018

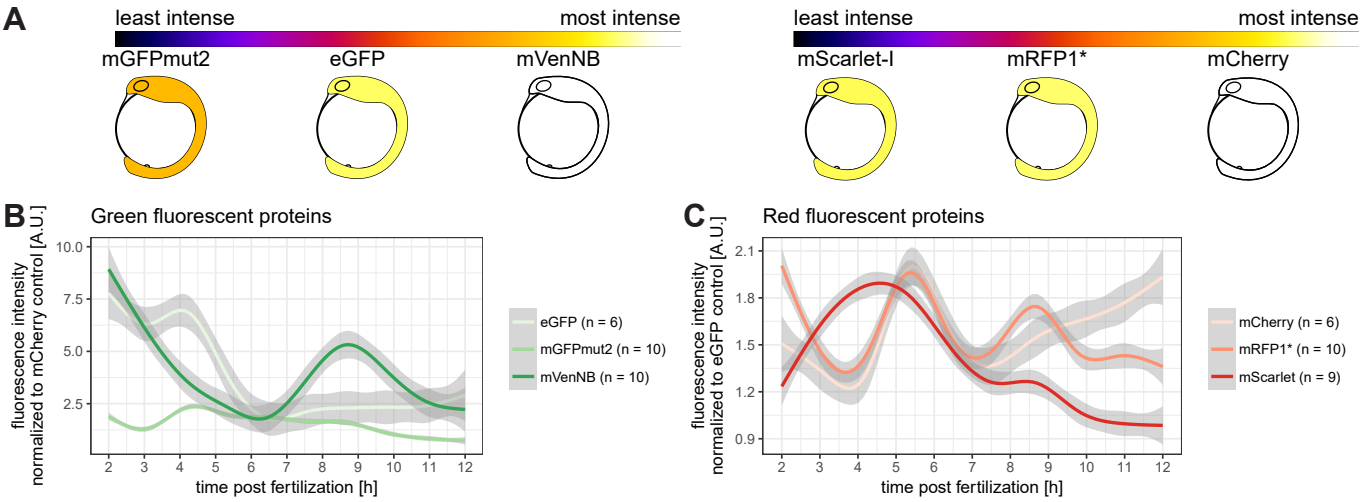

Fig 3, Lischik et al. 2018

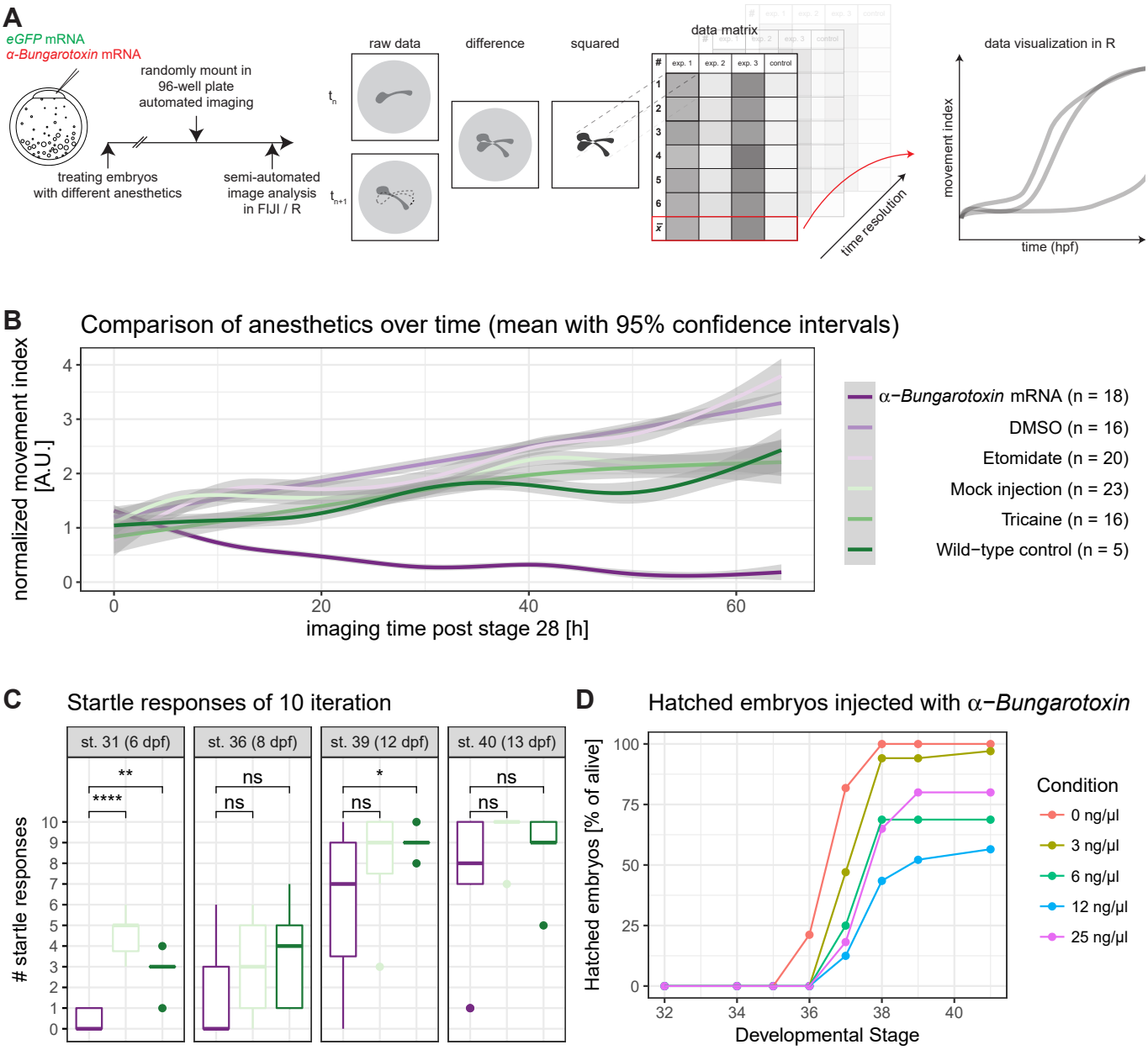

Fig 4, Lischik et al. 2018

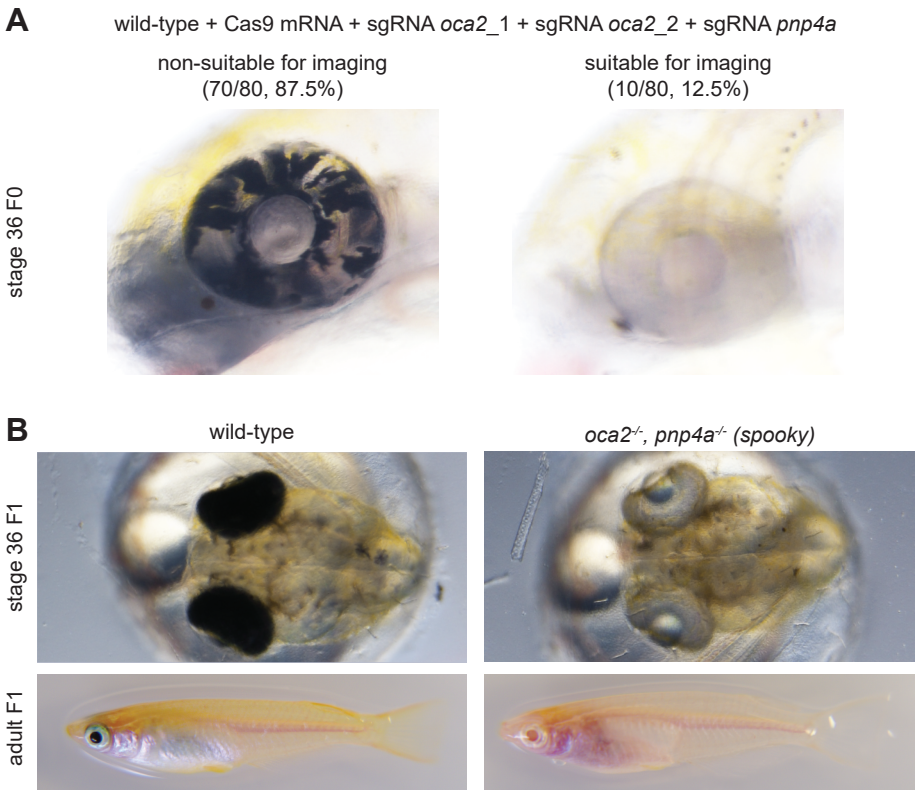

Fig 5, Lischik et al. 2018

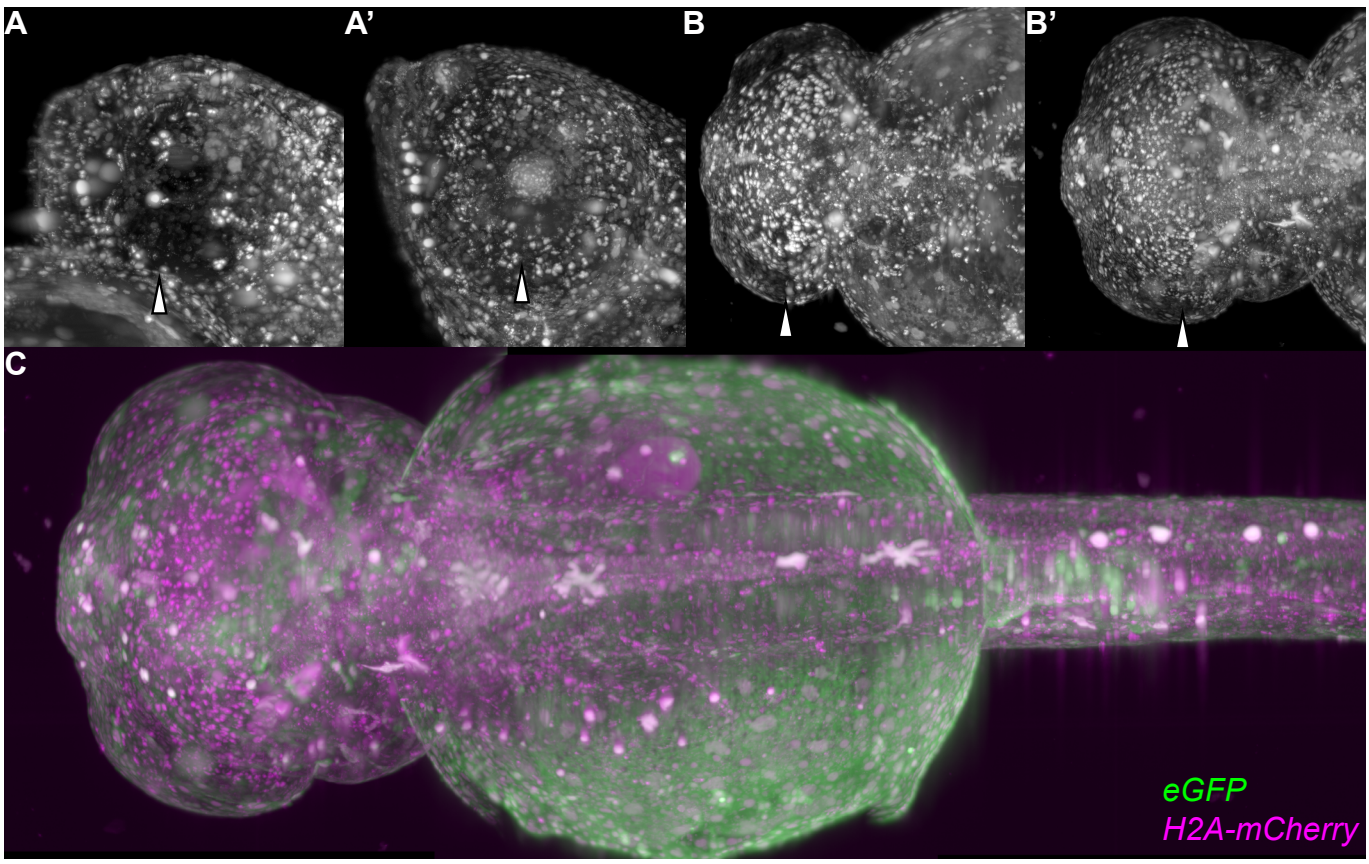

Fig 6, Lischik et al. 2018